Phase composition and surface properties of nylon-6 nanofibers prepared by nanospider technology at various electrode distances

Article *in* Journal of Polymer Research · June 2015

DOI: 10.1007/s10965-015-0741-3

CITATIONS
8

READS
247

8 authors, including:

Pavla Capkova
Jan Evangelista Purkyně University
153 PUBLICATIONS **1,975** CITATIONS
SEE PROFILE

Martin Kormunda
Jan Evangelista Purkyně University
91 PUBLICATIONS **1,182** CITATIONS
SEE PROFILE

Jaroslav Pavlík
Jan Evangelista Purkyně University
39 PUBLICATIONS **282** CITATIONS
SEE PROFILE

Marcela Munzarová
Nanovia s.r.o.
50 PUBLICATIONS **493** CITATIONS
SEE PROFILE

J Polym Res (2015) 22: 101
DOI 10.1007/s10965-015-0741-3

ORIGINAL PAPER

Phase composition and surface properties of nylon-6 nanofibers prepared by nanospider technology at various electrode distances

Pavla Čapková[1] · Antonín Čajka[1] · Zdenka Kolská[1] · Martin Kormunda[1] · Jaroslav Pavlík[1] · Marcela Munzarová[2] · Milan Dopita[3] · David Rafaja[3]

Received: 4 January 2015 / Accepted: 20 April 2015 / Published online: 7 May 2015

Abstract Phase composition, morphology and surface properties of nylon-6 nanofibers prepared by *Nanospider* technology have been studied for dependence on spinning distance using a combination of X-ray diffraction (XRD), X-ray photoelectron spectroscopy (XPS), electrokinetic analysis, and scanning electron and transmission electron microscopy (SEM, TEM). The effect of the electric field strength on the nanofiber phase composition was investigated via the variable distance of the electrodes. Quantitative XRD phase analysis revealed the dependence of the phase composition on the electrode distance, which in the case of roller electrospinning, differs from that by melt spinning. A combination of XRD, XPS, and TEM suggested a core-shell structure model of the nanofibers. The XPS and electrokinetic analysis revealed the difference in surface chemistry and zeta potential at the face and reverse side of the nanofiber textile adjacent to a polypropylene (PP) antistatic spunbond, which may be important in subsequent chemical modification of nanofiber textiles and in its use for tissue engineering.

Keywords Nylon-6 · Nanofiber textile · Phase composition · Structure model · Zeta potential

✉ Pavla Čapková
Pavla.Capkova@ujep.cz

[1] Faculty of Science, University of J. E. Purkyně , České mládeže 8, CZ-40096 Ústí nad Labem, Czech Republic

[2] Nanovia, s.r.o., Litvínov, Podkrušnohorská 271, CZ-436 03 Litvínov-Chudeřín, Czech Republic

[3] Institute of Materials Science, TU Bergakademie Freiberg, Gustav-Zeuner-Str. 5, D-09599 Freiberg, Germany

Introduction

Polymer nanofibers find use in a wide range of areas such as filtration [1–5], protective clothing, pharmaceuticals [6–8], tissue engineering [9–11], etc. Among all polymeric fibers, nylon-6 attracts the greatest attention due to its extraordinary properties: biodegradability, biocompatibility, and good mechanical properties [12]. Various experimental arrangements and equipment have been described in the literature for spinning of nylon-6 nanofibers either by melt spinning using an extruder attached to a pump, see for example [13, 14], or by electrospinning with a syringe attached to a capillary tip connected to the positive electrode [1, 15, 16]. Morphology and structure of the fibers prepared by these techniques have been characterized by dependence on spinning conditions and technology parameters [1, 13–18]. However, the structure of fibers prepared by *NANOSPIDER* technology, i.e., the roller spinning is less studied [19], although this technology is industrially used and important in practice. This study is devoted to the structure, phase composition, and surface properties of nylon 6 nanotextile prepared by *NANOSPIDER* technology.

It is well known that nylon-6 is polymorphic, having the following crystal structures: (1) The α- form described by Brill [20] and Holmes et al. [21] and (2) the γ-form determined by Holmes et al. [21] and later by Arimoto et al. [22]. Both structures are monoclinic and differ from each other in the arrangement of polymeric chains, in the density and cohesive energy, and, consequently, in their physical and chemical properties. Roldan and Kaufman [23] pointed out that nylon-6 can also form an amorphous structure, a disordered α-phase, and a disordered γ-phase, which are described as nematic, smectic, and paracrystalline, respectively. The effect of crystallization conditions on the formation of the α-phase versus γ-phase has been widely studied [24–33] and led to the

following general conclusions: rapid cooling or quenching from the melt and low crystallization temperature produce preferentially the γ-phase, while the higher crystallization temperatures or slow cooling lead to the α-phase.

In electrospun nanofibers, both phases α and γ usually coexist with an amorphous phase [1, 2, 13, 14, 16, 17]. Their volume fraction depends on the spinning conditions. Samon et al. [14] and Penning et al. [17] investigated the dependence of the volume fraction of both crystalline phases and of the amorphous phase on the take-up speed. They showed that the α-phase is formed at lower cooling rates and that the γ-phase occurs at higher take-up speeds. The volume fraction of amorphous phase increases with increasing take-up speed. All these structural studies have been carried out for nanofibers prepared either by melt spinning or by capillary (needle) electrospinning. In this study, we analyze the nanofiber nonwoven textiles prepared by roller electrospinning - *NANOSPIDER* technology.

There are many factors affecting the morphology and phase composition of nylon-6 nanofibers, the phase composition always depends on the cooling rate. It is well known that the α-phase with higher density needs a longer crystallization time than the γ-phase, which has more loosely packed chains. The cooling rate can be controlled by the take-up speed, spinning distance, and electrode voltage. In the present work we use the spinning distance for the control of the cooling rate.

NANOSPIDER is a modified electrospinning, where the roller electrospinning device contains a roller spinning electrode partially immersed in a tank with the polymer solution. A grounded collector electrode is placed at the top of the spinner. Roller electrospinning enables production of nanofibers from a thin layer of liquid polymer [34, 35]. Yener and Jirsak [35] compared the morphology and fiber diameter of polyvinylbutyral for the needle and roller electrospinning and showed that the needle electrospinning results in nanofibres of smaller diameters. On the other hand, roller electrospinning shows a considerably greater throughput.

The present work is focused on the investigation of properties important for practical applications of nanotextiles prepared by roller electrospinning like phase composition and zeta potential. The phase analysis using X-ray diffraction is extremely difficult due to the high degree of structural disorder, small size of crystallites, the presence of an amorphous phase, and strong texture in nanofiber textile samples that are furthermore difficult to handle for preparation. The structure and phase composition are parameters affecting the thermal, mechanical, and surface properties,and; therefore, we paid special attention to XRD data analysis. The combination of XRD with further techniques—SEM, TEM, XPS, and electrokinetic measurements has been used for the complete characterization of nylon-6 nanofiber textiles prepared by *NANOSPIDER* technology.

Experimental

Materials and technology

Granules of nylon-6 (Ultramid B24 N03) purchased by BASF were dissolved by gentle stirring for 24 h at 65 °C in a 2:1 solution of acetic acid and formic acid in order to prepare 12w% solution. Electrospinning was carried out using a Nanospider laboratory machine NS 1WS500U from Elmarco at room temperature (24.5 °C), driving voltage 90 kV, and at a humidity of 41.3 %. The distance between the active electrode and the collecting electrode was varied: 150, 200, 250, and 300 mm (samples: S150, S200, S250 and S300).

The nanofibers produced were collected on the polypropylene (PP) antistatic spunbond nonwoven backing material moving along the collector electrode at a constant velocity of 0.18 m/min.

Characterization of textile samples

Microstructure and phase composition of electrospun textile sheets has been analyzed by X-ray diffraction (XRD analysis) using a Philips PANanalytical powder diffractometer X;pert PRO in symmetrical reflection mode with the CuKα radiation (<λ>=1.5418 Å), Ni filter located in the primary beam and a PIXcel^{3D} detector. Flat samples for the symmetrical reflection mode were prepared by successive layering and compression of nanofiber nylon-6 sheets. A SEM microscope, Tescan Vega II (operating at 30 kV), was used to show the relation between the microstructure and morphology of nanofibers.

The surface characterization was performed by the XPS (X-ray photoelectron spectroscopy) technique. The high vacuum chamber was equipped with a source SPECS X-Ray XR50, where an Al cathode (1486.6 eV) was used, and with a hemispherical analyzer, SPECS PHOIBOS 100, with a 5-channels detector. The pressure before measurement was about $3*10^{-9}$ mbar in the instrument.

Surface chemistry and polarity of nanofiber surfaces were determined using electrokinetic analysis. The zeta potential of tested surfaces was accomplished on a SurPASS Instrument (Anton Paar, Austria). Samples were studied inside the adjustable gap cell in contact with the electrolyte (0.001 mol dm^{-3} KCl) at room temperature. For each measurement, a pair of polymer samples with the same top layer was fixed on two sample holders (with a cross section of 20×10 mm^2 and a gap between 100 μm). All the samples were measured four times at constant pH (pH=6.4) with a relative error less than 5 %. For determination of the zeta potential, the streaming current and streaming potential methods were used and the Helmholtz–Smoluchowski and Fairbrother-Mastins equations were applied to calculate the zeta potential [36].

The TEM analysis was performed on a 200 kV analytical high-resolution transmission electron microscope JEM 2200

FS from Jeol. The diffraction contrast was employed for the local analysis of the phase composition. For the TEM analysis, the samples were embedded in synthetic resin and cut in slices by using an ultramicrotome. In order to enhance the electrical conductivity of the TEM sample and to improve its stability in the primary electron beam, the slices on the grid were coated by a few nanometers of carbon.

Results and discussion

Phase and microstructure analysis

Figure 1 shows the calculated powder diffraction patterns for ideal crystal structures of the α and γ phases of nylon-6 having no preferred orientation of crystallites. The diffraction patterns were simulated in a *Materials Studio* [37] modeling environment using the module *Reflex*. The slight line broadening in the calculated diffraction pattern was achieved via the crystallite size of 50 nm and by a small lattice strain due to the structural disorder (ε=0.01 %). The diffraction pattern of the starting material (nylon-6 granules) is shown in the Fig. 2. It resembles the diffraction pattern calculated for the α-phase; the strong reflections 200 and 002 dominate the diffraction profile. This means that the α-phase is prevailing in the initial granulated material.

Development of the diffraction profiles of a nanofiber textile is dependent on the electrode gap for distances: 150, 200, 250 and 300 mm are in Fig. 3. Figure 4 illustrates the decomposition of the overall profile for the sample S150. The analysis of the XRD pattern of sample S150 confirmed the coexistence of both phases α and γ. Whereas the existence of the γ phase is proven by the main reflection 200 at 2θ=21.55°, the presence the of α-phase manifests itself by the shoulders on only the diffraction profile. These shoulders correspond to the reflections 200 at 2θ=20.11° and 002 at 2θ=24.05°.

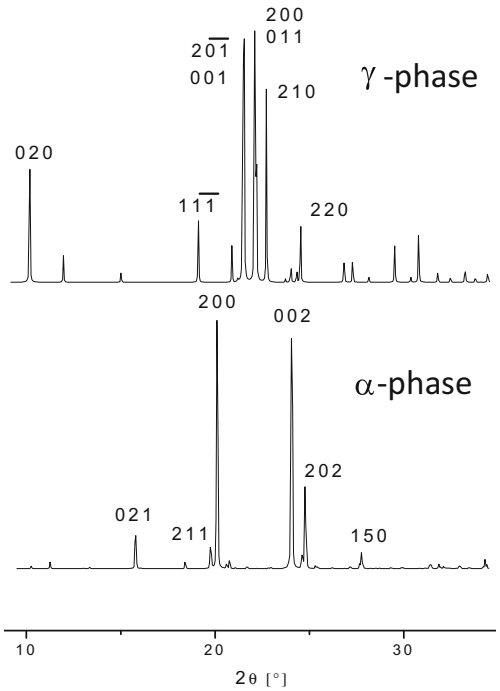

Fig. 1 Powder diffraction patterns calculated for the ideal crystal structures of the phase α (the *lower* diagram) and the phase γ (the *upper* diagram)

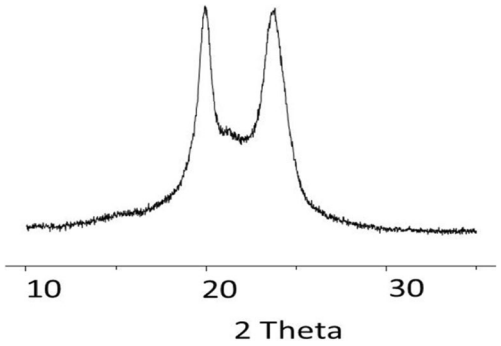

Fig. 2 Diffraction pattern of the starting material—nylon-6 granules

The absence of the strong reflection 020 of the γ-phase (cf. Fig. 1) suggests a strong crystallographic texture. This means that the crystallographic direction ⟨010⟩, which is the direction of the molecular axis, is preferentially oriented to the fiber axis. As the fibers are lying flat in the sample, the ⟨010⟩ direction is perpendicular to the diffraction vector if the measurement is performed in symmetrical diffraction geometry. Consequently, the (020) crystallographic planes, which are oriented perpendicularly to the fiber axis, are perpendicular to the textile plane. Thus, they have no chance to attain the diffraction position. For this reason, the relatively strong reflection (020) at~10.5° (see the theoretical diffractogram in Fig. 1) is

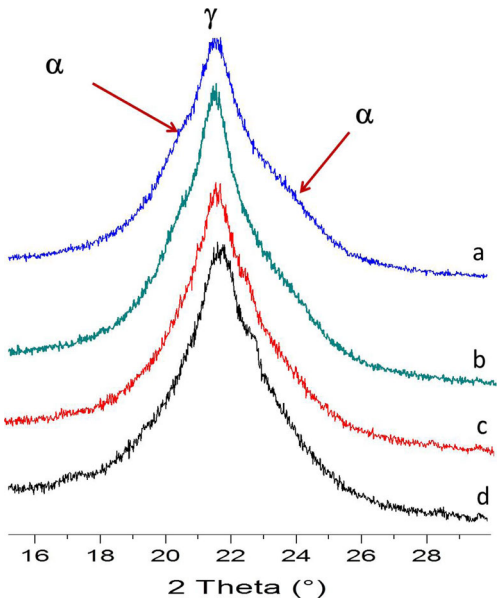

Fig. 3 Development of the diffraction profiles is dependent on the electrode gap for distances: 150, 200, 250, and 300 mm

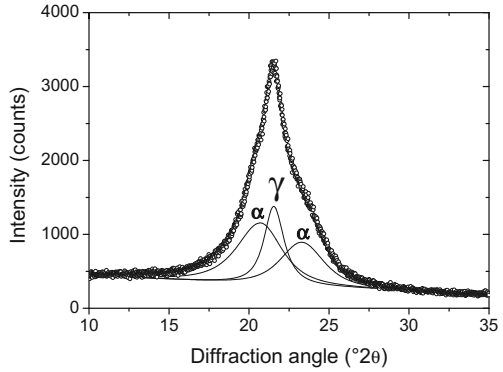

Fig. 4 Observed diffraction pattern for the sample S150 with the electrode gap of 150 mm (*small circles*). The diffraction lines from the individual phases (*solid lines*) were obtained by fitting the measured intensities by three Pearson VII functions [38] and are labelled by diffraction indices. Only the line profiles corresponding to the spectral line $CuK_{\alpha 1}$ are shown

missing in the observed diffraction pattern. An analogous result was obtained for the α-phase, which did not provide the diffraction lines *hkl* with a non-zero index *k* in the symmetrical diffraction geometry as well, because the corresponding lattice planes cannot be parallel to the sample surface for such oriented fibers, and; therefore, they do not diffract.

The decomposition of the XRD pattern into these three diffraction lines revealed that the XRD lines 200 and 002 from the α-phase are much broader than the XRD line 200 from the γ-phase in all measured samples. This difference in the XRD line broadening indicates that the coherently diffracting domains (crystallites) are smaller in the α-phase than in the γ-phase. Furthermore, the decomposition of the XRD pattern provided the integral intensities of the individual diffraction lines that were employed for semi-quantitative phase analysis.

Assuming that all fibers are lying flat in the samples but randomly rotated around the fiber axes, the intensities of the observed reflections, i.e., 200 and 002 from the α-phase and 200 from the γ-phase, are unaffected by the supposed texture. Therefore, the intensities of individual reflections can be compared with the corresponding calculated intensities as usual,

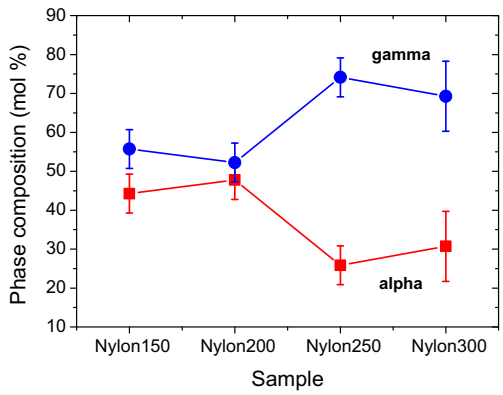

Fig. 5 The phase composition of the electrospun fibers as a function of the distance between the active electrode and the collecting electrode

e.g., in the Rietveld method [39]. Neglecting the absorption of X-rays within the fibers, the intensity ratios correspond to the molar ratio between the α- and γ-phase. Independent of the distance between the electrodes, the amount of the γ-phase was larger than the amount of the α-phase. The phase composition obtained by the XRD profile analysis of the electrospun fibers as a function of the distance between the active electrode and the collecting electrode is shown in Fig. 5. It is evident that the nylon-6 nanofibers prepared by *NANOSPIDER* technology consist predominantly of the γ-phase for all electrode distances and the content of the α-phase is lower than in fibers prepared by melt spinning as reported in [14, 17].

For the small electrode distances 150 and 200 mm, the content of γ- phase is slightly higher than the content of α-phase. At larger distances for the electrodes, the amount of the γ-phase increased significantly, while the amount of the α-phase decreased. The relatively high content of the α-phase for the short electrode distance is probably a consequence of the nylon chains arrangement in the spinning solution. The starting material,nylon-6 granules, which exists in α-phase, keeps, to a certain extent, the ordering arrangement of chains in the spinning solution. Consequently, in the electrospun nanofibers at the early stage of spinning - for the very short electrode distances - they keep the arrangement of chains from the spinning solution. The XRD lines from the α-phase were always wider than the XRD lines from the γ-phase, indicating much smaller crystallites in the case of the α-phase, than for the γ-phase, as it is illustrated in Fig. 4. This result is consistent with the previous findings that the α-phase needs the higher temperatures and slow cooling for crystallization. Table 1 summarizes the volume fraction of the amorphous phase, obtained using the program Highscore (http://www.panalytical.com/Xray-diffraction-software/HighScore.htm).

XPS analysis

The XPS analyses were performed on the raw material (nylon-6 granules) and nanotextile samples. The elemental composition of a nanotextile is similar on both sides (face side and reverse side adjacent to the spunbond) and does not change with spinning conditions (see Table 2). The elemental composition of the surface layer for raw material - PA6 granules are slightly different from that of nanotextiles, as one can see in Table 2. This difference between nanotextiles and granular

Table 1 The volume fraction of the amorphous phase for samples prepared with electrode gaps of 150, 200, 250, and 300 mm

Sample	S150	S200	S250	S300
Electrode distance [mm]	150	200	250	300
Volume fraction of amorphous phase [%]	17	13	11	9

Table 2 Elemental composition of nylon-6 granules and nanofiber textiles determined by XPS

	Atomic concentration [%]		
Element	C	N	O
Granules nylon-6	80.1	9.0	10.9
Nanotextile (face side)	75.6	12.5	12.0
Nanotextile (reverse side)	76.2	11.8	12.0

samples is not surprising, as the XRD analysis revealed different phase compositions in both type of samples. In addition α-phase, which is predominant in granules, has a higher density than the γ-phase dominant in nanotextile samples. No other elements were identified in the spectra.

The high resolution X-ray photoelectron spectra of C 1s and N 1s have a practically identical shape when normalized, as one can see in Figs. 6 and 7. The carbon peaks are composed of three peaks similar to the literature [40]: C1 at 284.5 eV corresponds to a C-C bond, C2 at a binding energy (BE) of 286.1 eV corresponding to a C-N bond and C3 at a BE of 287.5 eV corresponding to an O=C-N bond (amide group). However, the high resolution of O 1 s spectra for raw PA6 granules composed mainly from the α-phase are significantly different from the O 1 s peak of nanotextiles composed mainly of the γ-gamma phase. As one can see in Fig. 8, the O 1 s peak for granules exhibits a pronounced shoulder at higher energies. The O 1 s spectra should be precisely formed only by an

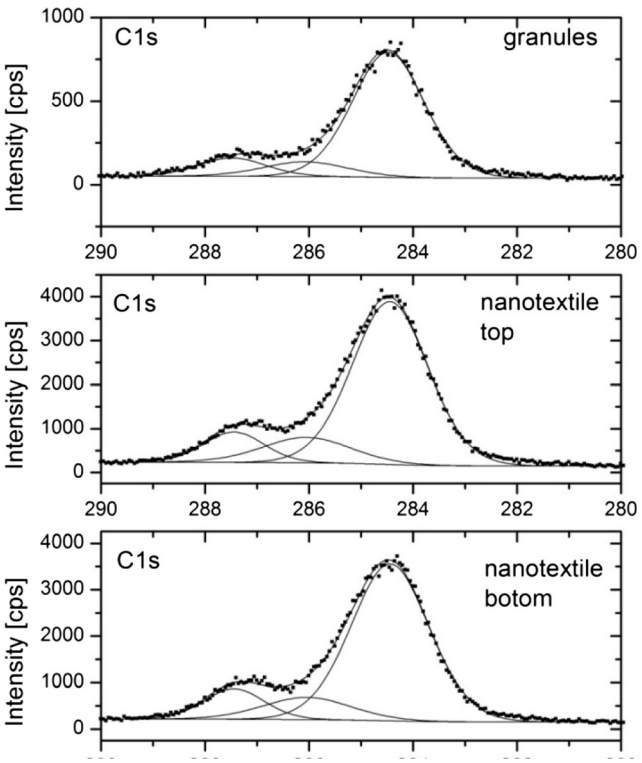

Fig. 6 The high resolution C1s peaks on granules and nanotextiles

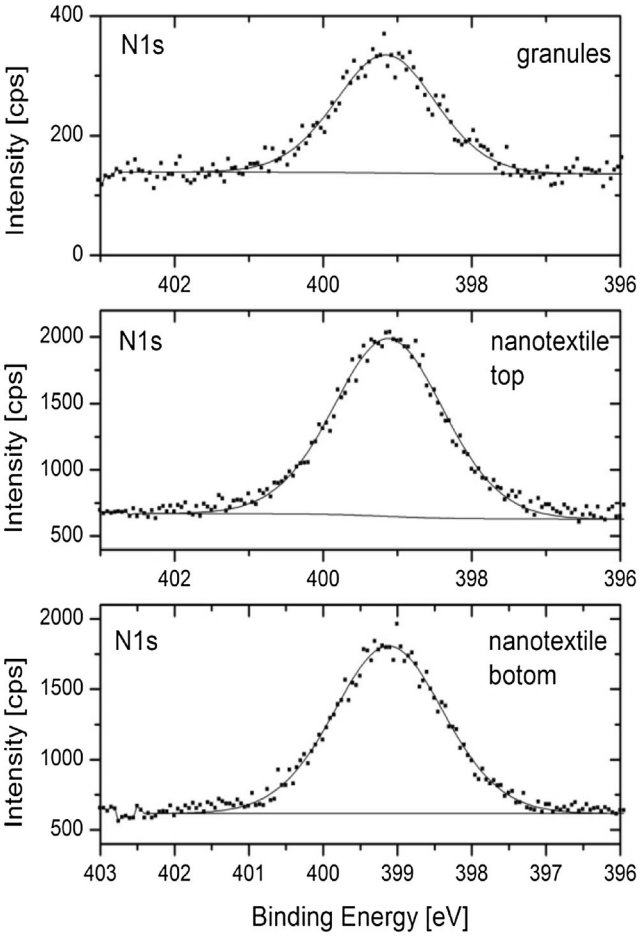

Fig. 7 The high resolution N1s peaks on granules and nanotextiles

O=C-N bond . It is important to point out that the binding energies are influenced by the chemical surrounding the bond; therefore, the identification of the bond by only BE leads to misinterpretation.

Figure 8 indicates that oxygen has different surroundings (i.e., a different crystallographic environment) in the structure of granules and nanotextiles. This is consistent with the result of XRD: granules are mainly composed of a α-phase, while a nanotextile is predominantly composed of a γ-gamma phase. Both of the structural phases α and γ have a lamellar arrangement of molecular chains; however, the mutual orientation of chains in lamellae is different, and that means different hydrogen bond schemes in the α and γ-phases. Hydrogen bonding is intra-sheet in the α and inter-sheet in the γ crystalline form [21, 22]. Analysis of the length of hydrogen bridges using structure data [21, 22] revealed that the γ-phase has one type of H-bonds with a H-O distance of 1.73 Å, whereas the α-phase possesses two types of H-bridges with the H-O distances of 1.74 and 2.04 Å, which means stronger H-bonds in the γ than in the α form. These structural differences explain the broadening of the XPS profile O1s peak observed for granules, which are composed mainly from the α-phase. This

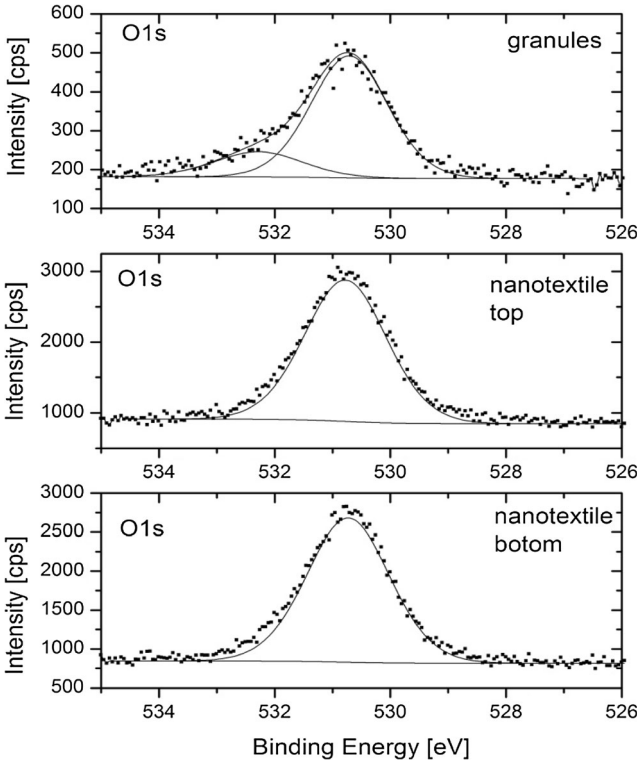

Fig. 8 The high resolution O1s peaks on granules and nanotextiles

is consistent with the results of the force field calculations [41] and results of [42].

Morphology of nanofibers studied by SEM and TEM analysis and structure models

Figure 9 shows scanning electron micrographs of samples S150 – S300 (a–d) with electrode distances of 150, 200, 250, and 300 mm. It is evident that increasing electrode distance resulted in better homogeneity and less defects on the fibers. With increasing electrode distance, the nanofiber textile becomes more homogeneous as to the fiber diameter. The fiber thickness inhomogeneity along the fiber axis has been observed to a certain extent for all samples. This may be due to the crystal grains boundaries, where we can expect a disorder in polymer chains resulting in an amorphous structure between the individual nylon-6 crystallites. TEM microscopy was used to investigate the structure of individual fibers in more detail. The TEM micrographs revealed the tendency to axial symmetry of the phase composition. One example is depicted in Fig. 10.

The combination of X-ray diffraction, XPS, SEM, and TEM analysis led us to the core-shell structure model schematically drawn in Fig. 11, where the shell is composed from the γ-phase and the core from the α-phase. Creating the structure model, we have to take into account also the presence of an amorphous phase, which may be naturally situated at the phase boundary along the fiber axis. Another amorphous region is located across the fibers at the grain boundaries.

The core-shell structure model is based on the following specific findings:

- XRD analysis confirmed the predominant α-phase in granules and the predominant γ-phase in nanofiber textile samples.
- XPS analysis providing information from surfaces showed the difference in oxygen O1s peaks for granules composed from the α-phase and nanotextiles composed of the γ-phase. This means that the surface of the nanofibers does not contain the α-phase.
- It is known that the γ-phase has lower density than the α-phase and TEM images show more bright regions mostly at the fiber shells (with some exceptions), as one can see in Fig. 10.
- It is also well known from many previous publications [24–33], that the γ-phase is formed during rapid cooling, while the α-phase needs slower cooling and a longer crystallization time. During the electrospinning we can expect much faster cooling in the fiber surface than in the core, consequently, conditions for the growth of the α-phase are very unfavorable in the shell part of fibers.

Zeta potential

Electrokinetic analysis of solid samples is a useful method for surface characterization of flat samples [43]. Especially its combination with XPS measurement gives complex information about the surface chemistry and polarity and about the presence of important functional groups on the surface. Table 3 presents the results for nanofiber textile sample S200. The zeta potential (ZP) was found to be the same (within the experimental accuracy) for all samples. ZP was measured for both sides of a nanofiber textile: face and reverse using two methods: streaming current and streaming potential [36]. Results are summarized in Table 3.

The zeta potential of the samples was quite high (a less negative value) in comparison with other polymers tested previously [36], which indicates a presence of positively charged functional groups on the surface. In the case of nylon, there are leading amino groups in this positively charged surface in a liquid surrounding. Very small deviations of determination indicate the high chemical homogeneity of tested samples. A slight difference between results obtained by both of the applied methods can be caused by a slightly variable roughness and morphology of tested surfaces [36].

An interesting result is the difference of zeta potential for the face and reverse side of a nanofiber textile, which exceeds the experimental error. The reverse side has a quite higher zeta potential. This may be due to the reorientation of functional

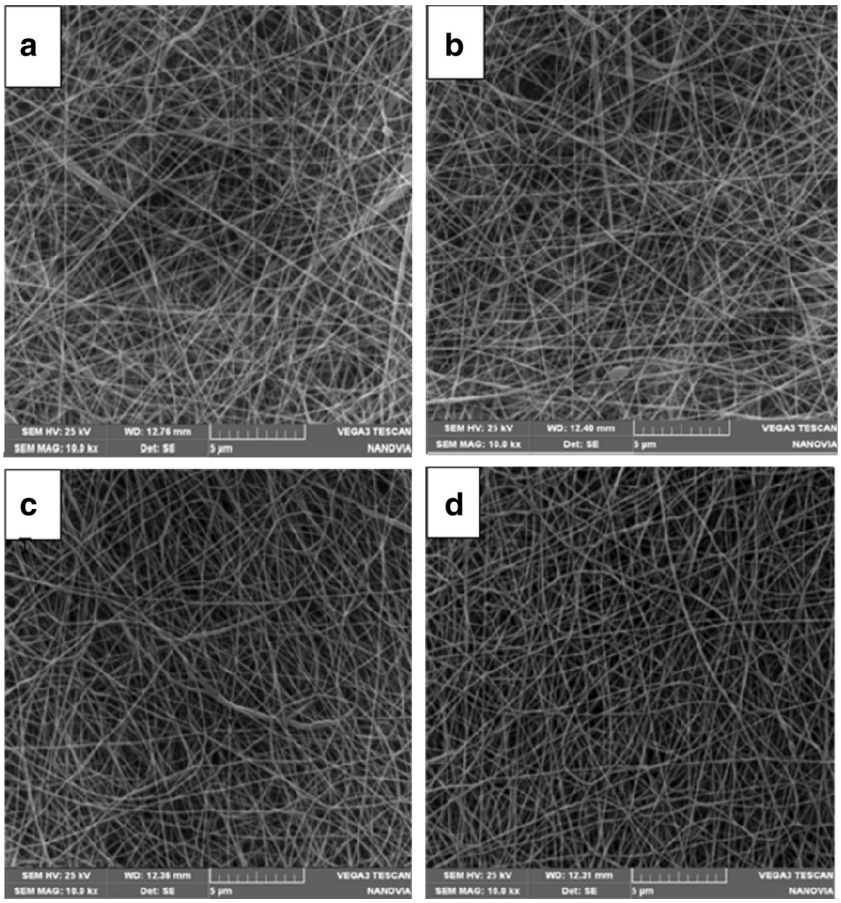

Fig. 9 Scanning electron micrographs of samples S150, S200, S250, and S300 for the following electrode distances: (**a**) 150 mm, (**b**) 200 mm, (**c**) 250 mm and (**d**) 300 mm. It is evident, that increasing electrode distance results in more homegeneous nanofibers diameter with less defects in the shape of beads. It is well seen from a comparison of images (**a**) and (**d**)

groups on the reverse side as a result of the interaction of a nanofiber textile with the spunbond. This is probably due to the spunbond being made from polypropylene (PP), which is a nonpolar polymer, functional groups of sprayed polar nylon have a tendency to reorient themselves to more polar surroundings. Therefore, the amount of nitrogen groups (positively charged amino groups) differ on both tested sides, which was confirmed by XPS measurement (see Table 2) and also by electrokinetic analysis (Table 3).

These results correspond very well. It was observed earlier, also for different polymers, that the surface properties vary depending on the tested side due to contact with surroundings during their manufacture [44, 45]. The quite high zeta potential value (about −10 mV), which clearly indicates the presence of positively charged functional groups on the surface, also confirms that the nylon textile is highly polar [36], and, due to this, it can strongly affect potential adhesion and proliferation of a living cell. It was presented earlier that the presence of amino groups on the surface significantly affects

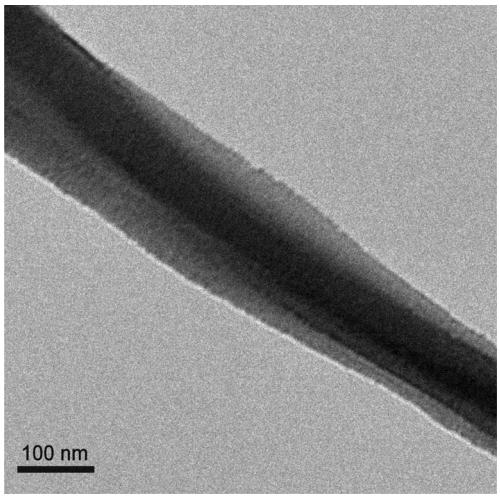

Fig. 10 The TEM micrograph of a single nanofiber confirming axial symmetry of the distribution of the crystalline phases

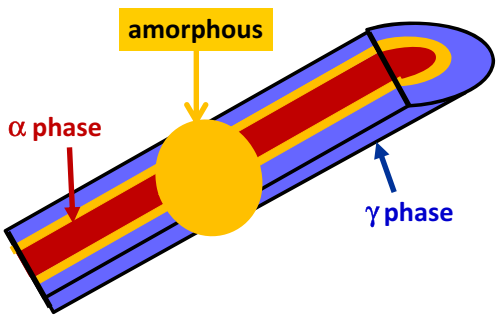

Fig. 11 The structure model of nylon-6 nanofibers schematically illustrating the distribution of individual phases

Table 3 Zeta potential (ZP) of nonwoven nanotextiles of nylon-6 for the face and reverse side of the textiles. HS means the streaming current method and the Helmholtz-Smoluchowski equation, FM means the streaming potential method and the Fairbrother-Mastin equation

Method	HS	FM
Sample side	ZP (mV)	ZP (mV)
Face	−14.32±0.33	−12.53±0.38
Reverse (adjacent to spunbond)	−13.20±0.26	−10.77±0.10

the adhesion and proliferation of vascular smooth muscle cells [46], human umbilical vein endothelial cells, [47] or for human fibroblasts [48]. These are probably, therefore, the major proteins (especially proteins of fetal bovine serum). Also, the cell membranes are negatively charged under physiological pH and the adsorbed proteins play a major role in the attachment of anchorage-dependent cells through their binding to integrins [48]. The adhesion of cells of negatively charged membranes can be facilitated by electrostatic interactions, and; therefore, better cell adhesion may be expected on positively charged surfaces [45, 48]. XPS and electrokinetic analyses provided the promising results of tested material with the surface chemistry and charge as hopeful materials for tissue engineering as the scaffold.

Conclusions

Nanofiber textiles of nylon-6 prepared by roller electrospinning have not been yet investigated in detail, although this technology is industrially utilized for a wide range of applications of nanofiber textile in nanofiltration and in biomedical engineering. Crystal structure is the fundamental characteristic that determines other properties. The phases α and γ of nylon-6 have different crystal structures that mean different arrangements of polymer chains and a different scheme of hydrogen bonding and consequently different physical, chemical, and especially surface properties. Therefore, the first task in the present investigation was not only the quantitative phase analysis of nylon-6 nanofiber textiles, but also the fiber nanostructure, i.e., the phase distribution in nanofibers.

The main results of the present work can be summarized by the following items:

1. *NANOSPIDER* technology provides different phase composition of nylon-6 nanofibers as compared to the melt spinning. This is due to the different precursors in both methods (1) dissolved α-phase granules in the *NANOSPIDER* spinning tank and (2) molten nylon-6 in case of melt spinning. The nylon-6 nanofibers prepared by *NANOSPIDER* technology consist predominantly of the γ-phase for all the electrode distances and the content of the α-phase is lower than in fibers prepared by melt spinning.
2. The core-shell structure model of nylon-6 nanofibers model that is based on the present experiments shows that the fiber surface always consists of a γ-phase, due to the more rapid cooling of the surface region. This result is consistent with the previous findings that the γ-phase arises during rapid crystallization.
3. Zeta potential and adhesion properties are significantly different for the face and reverse sides of nanofiber textiles adjacent to the spunbond, due to the interaction of positively charged amino groups with polypropylene spunbond.
4. SEM analysis showed better fiber homogeneity and less faults for a higher spinning distance.

Increasing electrode distance led to an increase of crystallinity, i.e., to a decrease of the amorphous phase content. Comparison of theoretical and experimental XRD intensities led to the identification of the texture type in fibers. The crystallographic direction ⟨010⟩, which is the direction of the molecular axis, is preferentially oriented in the fiber axis. Nanofibers exhibit a strong texture for all the spinning distances and for both phases α and γ. Due to the high degree of preferred orientation, the reflections from crystallographic planes perpendicular to the fiber axis completely disappeared from the diffraction pattern. The results obtained by XPS and electrokinetic analyses, especially the difference between the face and reverse sides of the nanofiber textile, indicate different behaviors for potential cells adhesion, what may be important for a subsequent chemical modification, and for biomedical use, especially for tissue engineering.

Acknowledgments This work was supported by the Czech Science Foundation, project No: 13-06609S.

References

1. Ant HR, Bajgai MP, Yi C, Nirmala R, Nam KT, Baek W, Kim HY (2010) Effect of successive electrospinning and the strength of hydrogen bond on the morphology of electrospun nylon-6 nanofibers. Colloids Surf A Physicochem Eng Asp 370:87–94
2. Sang Y, Gu Q, Sun T, Li F, Liang CJ (2008) Filtration by a novel nanofibers membrane and aluminia adsorption to remove copper(II) from groundwater. J Hazard Mater 153:860–866
3. Yun KM, Hogan CJ, Matsubayashi Y, Kawabe M, Iskandar F, Okuyama K (2007) Nanoparticle filtration by electrospun polymer fibers. Chem Eng Sci 62:4751–4759
4. Nova CJM, Jeanjean DP, Belleville MP, Barboiu M, Rivallin M, Rio G (2008) Elaboration, characterization and study of a new hybrid chitosan/ceramic membrane for affinity membrane chromatography. J Membr Sci 321:81–89

5. Vitchuli N, Shi Q, Nowak J, Cord MM, Bourham M, Zhang X (2010) Electrospun ultrathin nylon fibers for protective applications. J Appl Polym Sci 116:2181–2187
6. Raghavan P, Zhao X, Kim JK, Manuel J, Chauhan GS, Ahn JH, Nan C (2008) Ionic conductivity and electrochemical properties of nanocomposite polymer electrolytes based on electrospun poly(vinylidene fluoride-co-hexafluoro-propylen) with nano-sized ceramics fillers. Electrochim Acta 54:228–234
7. Guo B, Zhao S, Han G, Zhang L (2008) Continuous thin gold films electroless deposited on fibrous mats of polyacrylonitrile and their electrocatalytic activity towards the oxidation of methanol. Electrochim Acta 53:5174–5179
8. Sill TJ, Recum HA (2008) Electrospinning: application in drug delivery and tissue engineering. Biomaterials 29:1989–2006
9. Kumbar SG, Nukavarapu SP, James R, Nair LS, Laurencin CT (2008) Electrospun poly(lactic acid-co-glycolic acid) scaffolds for skin tissue engineering. Biomaterials 29:4100–4107
10. Zhang Y, Venugopal JR, Turki AE, Ramakrishna S, Su B, Li CT (2008) Electrospun biomimetic nanocomposite nanofibers of hydroxyapatite/chitosan for bone tissue engineering. Biomaterials 29:4314–4322
11. Park SH, Kim TG, Kim HC, Yang DY, Park TG (2008) Development of dual scale scaffolds via direct polymer melt deposition and electrospinning for application in tissue regeneration. Acta Biomater 4:1198–1207
12. Sohrabi A, Shaibani PM, Thundat T (2013) The effect of applied electric field on on the diameter and size distribution of electrospun nylon6 nanofibers. Scanning 35:183–188
13. Fornes TD, Paul DR (2003) Crystallization behavior of nylon 6 nanocomposites. Polymer 44:3945–3961
14. Samon JM, Schultz JM, Wu J, Hsiao B, Yeh F, Kolb R (1999) Study of the structure development during the melt spinning of nylon 6 fiber by on-line wide-angle synchrotron x-ray scattering techniques. J Polym Sci Part B-Polym Phys 37:1277–1287
15. Zhang S, Shim WS, Kim J (2009) Design of ultra-fine nonwovens via electrospinning of Nylon 6: spinning parameters and filtration efficiency. Materials 30:3659–3666
16. Dersch R, Liu T, Schaper AK, Greiner A, Wendorff JH (2003) Electrospun nanofibers: internal structure and intrinsic orientation. J Polym Sci A Polym Chem 41:545–553
17. Penning JP, Ruiten JV, Brouwer R, Gabriëlse W (2003) Orientation and structure development in melt-spun Nylon-6 fibres. Polymer 44:5869–5876
18. Hussain D, Loyal F, Greiner A, Wendorff JH (2010) Structure property correlations for electrospun nanofiber nonwovens. Polymer 51:3989–3997
19. Deyab SSA, Newehy MHE, Nirmala R, Megeed AA, Kim HY (2013) Preparation of nylon-6/chitosan composites by nanospider technology and their use as candidate for antibacterial agents. Korean J Chem Eng 30:422–428
20. Brill R (1943) Crystal structure of nylon 6. Z Physik Chem B 53:61–66
21. Holmes R, Bunn CW, Smith DL (2003) The crystal structure of polycaproamide: Nylon 6. J Polym Sci A Polym Chem 17:159–177
22. Arimoto H, Ishibashi M, Hirai M, Chatani YJ (1965) Crystal structure of gamma-form of nylon 6. Polym Sci Part A 3:317–326
23. Roldan LG, Kaufman HS (1963) Crystallization of nylon 6. J Polym Sci B 1:603–608
24. Illers KH, Haberkorn H (1971) Specific volume, heat of fusion and crystallinity of nylon-6.6 and nylon 8. Makromol Chem 146:267–274
25. Gurato G, Fichera A, Grandi FZ, Zannetti R, Canal P (1974) Crystalinity and polymorphism of 6-polyamide. Makromol Chem 175:953–975
26. Kyotani M, Mitsuhashi S (1972) Studies on crystalline forms of nylon 6. II. Crystallization from the melt. J Polym Sci, Part A-2 10:1497–1508
27. Murthy NS, Aharoni SM, Szollosi AB (1985) Stability of the γ form and the development of the α form in nylon 6. J Polym Sci Polym Phys 23:2549–2565
28. Murthy NS, Curran SA, Aharoni SM, Minor H (1991) Premelting crystalline relaxations and phase-transitions in nylon-6 and 6,6. Macromolecules 24:3215–3220
29. Ramesh C, Gowd EB (2001) High-temperature X-ray diffraction studies on the crystalline transitions in the alpha- and gamma-forms of nylon-6. Macromolecules 34:3308–3313
30. Lincoln DM, Vaia RA, Wang ZG, Hsiao BS, Krishnamoorti R (2001) Temperature dependence of polymer crystalline morphology in nylon 6/montmorillonite nanocomposites. Polymer 42:9975–9985
31. Salem DR, Moore RAF, Weigmann HD (1987) Macromolecular order in spin-oriented nylon-6 (polycaproamide) fibers. J Polym Sci Part B: Polym Phys 25:567–589
32. Campoy I, Gomez MA, Marco C (1998) Structure and thermal properties of blends of nylon 6 and a liquid crystal copolyester. Polymer 39:6279–6288
33. Okada A, Kawasumi M, Tajima I, Kurauchi T, Kamigaito O (1989) A solid state NMR study on crystalline forms of nylon 6. J Appl Polym Sci 37:1363–1371
34. Jirsak O, Petrik S (2012) Recent advances in nanofibre technology: needleless electrospinning. Int J Nanotechnol 9:836–845
35. Yener F, Jirsak O (2012) Comparison between the needle and roller electrospinning of polyvinylbutyral. J Nanomater 2012:1155–1161
36. Kolská Z, Řezníčková A, Švorčík V (2012) Surface characterization of polymer foils. e-Polymers: Article 083:1
37. Materials Studio Accelrys Softrware Inc. (2007) http://accelrys.com/products/materials-studio/visualization-and-statistics-software.html
38. Hall MM Jr, Veerarghavan VG, Rubin H, Winchell PG (1977) J Appl Cryst 10:66–68
39. Rietveld HM (1967) Line profiles of neutron powder-diffraction peaks for structure refinement. Acta Cryst 22:151–152
40. Vesel A, Mozetic M, Strnad S, Persin Z, Stana-Kleinschek K, Hauptman N (2009) Plasma modification of viscose textile. Vacuum 84:79–82
41. Li YY, Goddard WA (2002) Nylon 6 crystal structures, folds, and lamellae from theory. Macromolecules 35:8440–8455
42. Liu Y, Li C, Guan F, Yi G, Hedin NE, Zhu L, Fong H (2007) Crystalline morphology and polymorphic phase transitions in electrospun nylon-6 nanofibers. Macromolecules 40:6283–6290
43. Švorčík V, Řezníčková A, Kolská Z, Slepička P, Hnatowicz V (2010) Variable surface properties of PTFE foils. e-Polymers Article 133: 1
44. Kolská Z, Řezníčková A, Hnatowicz V, Švorčík V (2012) Surface properties of poly(ethylene terephthalate) foils of different thicknesses. J Mater Sci 47:6429–6435
45. Kolská Z, Řezníčková A, Nagyová M, Slepičková Kasálková N, Sajdl P, Slepička P, Švorčík V (2014) Plasma activated polymers grafted with cysteamine improving surfaces cytocompatibility. Polym Degrad Stabil 101:1–9
46. Arima Y, Iwata H (2007) Effect of wettability and surface functional groups on protein adsorption and cell adhesion using well-defined mixed self-assembled monolayers. Biomaterials 28:3074–3082
47. Faucheux N, Schweiss R, Lutzow K, Werner C, Groth T (2004) Self-assembled monolayers with different terminating groups as model substrates for cell adhesion studies. Biomaterials 25:2721–2730
48. Sirmerová M, Procházkova G, Siristova L, Kolská Z, Branyik T (2013) Adhesion of Chlorella vulgaris to solid surfaces, as mediated by physicochemical interactions. J Appl Phycol 25:1687–1695